THE JOURNAL OF BIOLOGICAL CHEMISTRY VOL. 286, NO. 23, pp. 20870–20879, June 10, 2011

Large Scale RNAi Screen Reveals That the Inhibitor of DNA Binding 2 (ID2) Protein Is Repressed by p53 Family Member p63 and Functions in Human Keratinocyte Differentiation*[S]

Received for publication, July 28, 2010, and in revised form, April 1, 2011 Published, JBC Papers in Press, April 10, 2011, DOI 10.1074/jbc.M110.169433

Ning Wu[‡§1], David Castel[‡1], Marie-Anne Debily[§¶1], Maria Alessandra Vigano[‖], Olivier Alibert[§], Roberto Mantovani[‖], Kristina Iljin[**], Paul-Henri Romeo[§], and Xavier Gidrol[‡§2]

*From the [‡]CEA, IRTSV, Laboratoire Biopuces, 17 rue des Martyrs, 38054 Grenoble cedex 9, France, [§]CEA, IRCM, Laboratoire d'Exploration Fonctionnelle des Génomes 2 rue Gaston Crémieux CP22, 91057 Evry Cedex, France, the [¶]Université d'Evry Val d'Essonne, Boulevard François Mitterrand, 91025 Evry Cedex, France, the [‖]Dipartimento di Scienze Biomolecolari e Biotecnologie. Universita' di Milano. Via Celoria 26, 20133 Milano, Italy, and the **Medical Biotechnology, VTT Technical Research Centre and University of Turku, Itäinen pitkäkatu 4C, Turku, Finland*

The inhibitor of DNA binding 2, dominant negative helix-loop-helix protein, ID2, acts as an oncogene and elevated levels of ID2 have been reported in several malignancies. Whereas some inducers of the *ID2* gene have been characterized, little is known regarding the proteins capable to repress its expression. We developed siRNA microarrays to perform a large scale loss-of-function screen in human adult keratinocytes engineered to express GFP under the control of the upstream region of *ID2* gene. We screened the effect of siRNA-dependent inhibition of 220 cancer-associated genes on the expression of the *ID2::GFP* reporter construct. Three genes *NBN*, *RAD21*, and *p63* lead to a repression of *ID2* promoter activity. Strikingly NBN and RAD21 are playing on major role in cell cycle progression and mitosis arrest. These results underline the pregnant need to silence *ID2* expression at transcript level to promote cell cycle exit. Central to this inhibitory mechanism we find p63, a key transcription factor in epithelial development and differentiation, which binds specific *cis*-acting sequence within the *ID2* gene promoter both *in vitro* and *in vivo*. P63 would not suppress ID2 expression, but would rather prevent excessive expression of that protein to enable the onset of keratinocyte differentiation.

ID2 is a member of the helix-loop-helix (HLH)[3] family of transcription factors (1–3). Proteins of the HLH family positively regulate transcription by binding to DNA via a basic domain, as either homodimers or heterodimers, and often drive cell lineage commitment and differentiation in various cell types. In contrast, the ID proteins (ID1, ID2, ID3, and ID4) lack the basic domain and associate instead with other members of the HLH family, preventing them from binding DNA. Thus, the ID proteins act as dominant negative regulators of bHLH. For instance, ID proteins interact with the E transcription factors, including E12, E47, and E2-2 (4), as well as members of the Ets family (5). Generally, ID proteins function as positive regulators of cell growth and as negative regulators of cell differentiation (6).

ID2 is the only member of the ID family which physically interacts with the retinoblastoma protein (RB). RB is actually an upstream regulator of the *ID2* gene, which in turn restrains the activity of ID2 (7). Although *ID2* is not a *bona fide* oncogene triggering transformation of normal cells after a genetic alteration, its overexpression seems to contribute to tumorigenesis by inhibiting cell differentiation and stimulating proliferation. Elevated levels of ID2 have been reported in several malignancies, such as pancreas carcinomas (8), breast cancer (9), neuroblastomas (10), prostate cancer (11), and lung cancer (12).

ID genes play an important role in controlling epidermal homeostasis and cell fate in human keratinocytes. We demonstrated that overexpression of ID2 in HaCaT cells induced their proliferation, while the siRNA-mediated depletion of ID2 resulted in cell cycle arrest (13). The anti-proliferative effect of retinoids on human keratinocytes seems to result from the down-regulation of *ID2* gene expression through a transcriptional convergence between Wnt and retinoid signaling (14). Transforming growth factor β (TGFβ) also inhibits growth of epithelial cells, including keratinocytes, through long term repression of *ID2* and *ID3* (15, 16). Similarly ID2 promotes tumor cell proliferation via control of cyclin D1 protein level (17). Finally, small enhancement of ID1 expression, but likely of other ID proteins as well, affects proliferation, differentiation, and apoptosis of keratinocytes grown in organotypic cultures (16).

Several genes, including some transcription factors, have been involved in the regulation of *ID2* expression. For example, *FSH* (18), *IGF1R* (19), β-catenin (20), and *MYC* (7) are inducers of *ID2*. *TGF*β seems to exert more subtle regulation, as it leads to repression of *ID2* in epithelial cells (15), while it acts as an inducer of *ID2* in immune cells (21). As *ID2* overexpression seems to affect key oncogenic pathways in cells, we sought to characterize more repressors of *ID2* expression.

RNA interference (RNAi) is a powerful approach to perform systematic loss-of-function screens. Several high-throughput

* This work was funded by CEA (to N. W. and D. C.), a fellowship from the "Fondation pour la Recherche Médicale" (to N. W.), and an Association pour la Recherche sur le Cancer (ARC) Fellowship (to D. C.).

[S] The on-line version of this article (available at http://www.jbc.org) contains supplemental Figs. S1–S3 and Tables S1–S3.

[1] These authors contributed equally to this study.

[2] To whom correspondence should be addressed. Tel.: 33438789796; Fax: 33438785917; E-mail: xavier.gidrol@cea.fr.

[3] The abbreviations used are: HLH, helix-loop-helix; RB, retinoblastoma protein; TSS, transcriptional start site.

phenotypic screens have been done in human cells using small interfering RNA (siRNA) libraries in a 96-well plate format. For instance, genes involved in TRAIL-induced apoptosis (22), cancer cell chemoresponsiveness (23), cell division (24), and haploinsufficiency diseases (25) have been recently characterized by large scale RNAi screens. Other groups have rather used large pools of small hairpin RNA (shRNA) using barcoded microarrays to analyze systematic loss-of-function in human cells (26–28). Here, we used siRNA microarrays (29) to perform a large-scale RNAi screen and characterize genes involved in the regulation of *ID2* expression. We monitored the effect of siRNA-dependent specific inhibition of 220 genes involved in cancer, in human keratinocytes stably expressing an *ID2* promoter::GFP reporter construct. We identified three new repressors of *ID2*. Specifically, we report that *NBN* and *RAD21*, two key actors of cell cycle checkpoint control (30–33) indirectly lead to repression of *ID2*, and that *p63*, a major regulator of skin development (34, 35), is a direct *ID2* repressor.

EXPERIMENTAL PROCEDURES

Cell Culture and Transfection—The non-tumorigenic, spontaneously transformed human keratinocyte cell line HaCaT (36) was obtained from CLS (Cell Line Service, Eppelheim, Germany). HaCaT cells were maintained at 37 °C in a 5% CO_2 humidified atmosphere in Dulbecco's modified Eagle's medium (DMEM) without calcium chloride containing GLUTAMAX, 4.5 g/liter glucose (Invitrogen), 10% fetal calf serum (Hyclone, Perbio Sciences, Erembodegem-Aalst, Belgium), 100,000 units/liter penicillin, and 50 mg/liter streptomycin (Invitrogen).

For the forward transfection experiments, keratinocytes were plated in 6-well plates and transfected the following day in complete medium containing 10 nM siRNA complexed to interferin (Polyplus Transfection, Illkirch, France). Cells were assayed 72 h after transfection. siRNA duplexes (control siRNA, AllStars Negative Control siRNA; p63 siRNA, SI00055118) were obtained from Qiagen (Hilden, Germany). TAp63γ (Addgene plasmid 14575), ΔNp63α (Addgene plasmid 14574) and the control plasmid pBABE-puro (Addgene plasmid 1764) were obtained from Addgene. The pRc/RSV plasmid was obtained from Invitrogen, and the plasmid pRc-Id2 was constructed as described in Ref. 13. Stable cell HaCaT cell lines expressing pRc-Id2 were generated through antibiotic selection.

Human primary keratinocytes were obtained from human mammary skin biopsy. Briefly, keratinocytes were isolated by overnight trypsinization in 0.5% trypsin (Invitrogen)/5% penicillin/streptomycin (Eurobio) in phosphate-buffered saline at 4 °C, followed by scraping with a scalpel; then cells were cultured in semi-defined KGM-2 medium (Clonetics) on flasks coated with collagen type I (Falcon Biocoat) at 37 °C and 5% CO_2. The differentiation program of secondary cultures was induced at confluency by a switch to the following differentiation medium: KBM-2 (Clonetics) supplemented with 0.5 mg/ml hydrocortisone, 5 mg/ml insulin, 5 ng/ml EGF, and 1.85 mM calcium.

ID2 Promoter and Plasmid Cloning—A DNA fragment of the *ID2* promoter region, spanning from −2046 bp upstream to +13 bp downstream of the TSS, was amplified by PCR on genomic DNA from HaCaT cells using flanking BamHI and KpnI restriction sequences for the forward and reverse primers, respectively (see supplemental Table S3 for primer sequences). The PCR was performed using high-fidelity DNA polymerase (Platinum HiFi Taq Polymerase, Invitrogen) according to the manufacturer's recommendations.

The PCR products were inserted into a modified pENTR™5′ (Gateway plasmid, Invitrogen) via TOPO-TA cloning technology (Invitrogen). Gateway recombination using pENTR5′-[ID2 promoter], pENTR-EGFP and the lentiviral backbone plasmid pLenti6/R4R2/V5-DEST was used to insert the *ID2* promoter region upstream of EGFP coding sequence following the manufacturer instructions (Invitrogen). The resulting lentiviral construct was verified by sequencing.

The promoter region (−2574 to ~+100 bp) was cloned into pENTR™5′ vector. Truncated ID2 promoters were PCR amplified and cloned into pENTR5′-TOPO vectors (PCR primers listed in supplemental Table S3). The pID2-Luc2P (pID2–2.7k, pID2–980, and pID2–329) vector was obtained using the MultiSite Gateway technology. Truncated *ID2* promoters were PCR amplified and cloned into pENTR5′-TOPO vectors (PCR primers listed in supplemental Table S3). The luciferase coding sequence (Luc2P ORF) was PCR-amplified from the pGL4.24 vector (Promega Madison, WI) using primer with *att*B flanking cassette, and inserted into the pDONR221 vector through a BP recombination. The reporter vector pID2-Luc2P was generated through LR recombination with pENTR5′-promID2, pENTR-Luc2P, and plenti6-R4R2-V5-DEST (Invitrogen).

Viral Production in HEK293-FT—Recombinant lentiviruses were produced by transient transfection of HEK 293FT cells according to the manufacturer's protocol (Invitrogen) with minor modifications. Lentivirus-containing supernatant was collected 48 h after transfection, 0.22 μm-filtered, and ultracentrifuged at 22,000 rpm for 90 min. The pellet was resuspended in 200 μl of phosphate-buffered saline and stored at −80 °C until the day of use.

Transduction and Cell Sorting—HaCaT cells were plated in 24-well plates and infected 12 h later in complete medium supplemented with 8 μg/ml protamine sulfate (Sigma-Aldrich) and diluted viral preparation to achieve the estimated range of multiplicity of infection (MOI) required. After 24 h, fresh medium was added and cells were cultured and passaged for several days. A subpopulation of pID2-HaCaT cells exhibiting homogeneous GFP expression was selected by two consecutive runs of FACS (MoFlo, Dako, Denmark) to increase sensitivity and allow measurement of subtle changes in GFP expression, in both direction.

siRNA Microarrays—siRNA were transfected into HaCaT cells using a reverse-transfection format as previously described (29) with slight modifications. Briefly, 0.5 μl of a 20 μM siRNA solution in 100 mM KoAc, 30 mM Hepes-KOH, 2 mM MgOAC pH 7.4 (Qiagen, Hilden, Germany) was mixed with 10 μl of PBS 1× (Invitrogen), 2 μl of 1.5 M sucrose solution (Sigma-Aldrich), and then 2 μl of Interferin transfection reagent (PolyPlus transfection, Strasbourg, France) and incubated 10 min at room temperature to allow for the formation of siRNA-Interferin complexes. Three microliters of a 1% (*w/v*) type B-gelatin solution (Sigma #G-1393) diluted in RNase-free water and 3 μl of Matrigel (BD Biosciences, Erembodegem,

Belgium) were added. After lipid/DNA complex formation with the transfection reagent, the mixture was arrayed in quadruplicate on Superfrost glass slides (Menzel-Gläser, Braunschweigm Germany) using a MicroGrid Compact microarrayer (Genomic Solutions, Cambridgeshire, UK) with 400 μm solid pins at 19 °C and 60% humidity. Each slide comprised 640 features, mainly corresponding to 150 distinct siRNA printed in quadruplicate, 16 negative controls (scrambled siRNA) and 16 positive controls (siGFP), ordered in twelve 8 × 8 blocks. Positive and negative control spots were scattered all over the microarray to take into account cell-seeding variability or local artifacts, to quality control the transfection efficacy and to establish a reference for GFP expression in transfected cells. After printing, the slides were stored at 19 °C in a desiccator until the day of use. Slides were transferred to fresh sterile 10-cm dishes, and cells were plated onto the slides in 10 ml of DMEM at $\sim 3 \times 10^5$ cells/cm^2. Cell microarrays were assayed 72 h after cell seeding. A minimum of three independent biological replicate experiments were carried out for each of the three batches of printed slides.

Immunofluorescence—Cells were fixed for 15 min in 4% (w/v) paraformaldehyde solution, washed 3 times in PBS and permeabilized for 5 min in a 0.1% (*v/v*) Triton X-100 solution (Sigma-Aldrich). Slides were then blocked in PBS-BSA 1% (w/v) for 30 min. EGFP expression was probed by immunostaining using Alexa647-coupled anti-GFP antibodies (1:250 dilution, Invitrogen) for 1 h at room temperature to increase the GFP signal. After several washes in PBS, nuclear DNA was then stained in a 0.25 μM Sytox Orange solution (Invitrogen) for 10 min. Slides were washed and dried, and independent fluorescence images of arrays were immediately captured using a Genepix 4000D microarray scanner (Molecular Devices) at 532 nm (PMT 200V) and 635 nm (PMT 550V) for DNA content and GFP expression staining, respectively.

siRNA Microarray Analysis—The fluorescence intensity values for each feature on the array were extracted using Genepix 4.0 (Molecular Devices). A .gal file (Genepix Array list) containing the coordinates of the different siRNA was generated before transfection and aligned on a pre-scan of the arrays to determine the precise localization of spots. After reverse-transfection, this grid was overlaid on the fluorescence images and used to extract the total intensity values corresponding to GFP (F_{total} 635) and DNA staining (F_{total} 532) of all cells in each feature (supplemental Fig. S1). A manual flagging of marginal spots (*i.e.* features comprising too few cells or dust) and regions of the slides with staining artifacts was performed and greatly improved the quality of the data (data not shown). For each spot, the ratio (F_{total} 635/F_{total} 532) or rGFP was computed. This ratio corresponds to the relative GFP expression (F635, represented in *green* in Fig. 1) related to the DNA content (F532, represented in *red* in Fig. 1). Thus, the ratio yields a GFP-fluorescence value normalized by the number of cells present in the spot. Data were then summarized to take into account intra-array replicates, and also replicate slides (inter-array replicates) (supplemental Fig. S1). Indeed, each siRNA was arrayed in quadruplicate on each slide, and three independent experiments were carried out. A total of 12 independent measures of the effect of a particular siRNA on *ID2* expression were obtained, revealing the reliability of the screening process. The median of rGFP was calculated and ranked for each array. siRNA having at least 3 unflagged replicates out of 4 were further considered in the analysis.

Semi-quantitative PCR (qRT-PCR)—One microgram of total RNA isolated with the RNeasy isolation kit (Qiagen) was reverse-transcribed using random primers and a SuperScript II reverse transcriptase (Invitrogen) according to the manufacturer's instructions. Quantitative PCR was carried out with the Platinum® qPCR SuperMix (Invitrogen) in an ABI 7500 Real-Time PCR System (Applied Biosystems) with 1/20th of the cDNA for each reaction (supplemental Table S3 for primer sequences). Assays were performed in triplicate. Data were transformed using the $2^{-\Delta\Delta Ct}$ formula (37). Changes in abundance of the tested (target) gene were normalized to the 18 S ribosomal RNA level (reference gene) and compared with the relative expression of a calibrator sample (control, siRNA scrambled transfection).

Western Blotting—Cells were lysed in RIPA buffer (Pierce) (25 mM Tris-HCl, pH 7.6, 150 mM NaCl, 1% sodium pyrophosphate, 1% sodium deoxycholate, 1% SDS) containing protease and phosphatase inhibitors (1 mM PMSF, 10 μg/ml aprotinin, 10 μg/ml leupeptin, 10 μg/ml pepstatin, 1 mM Na3VO4, 50 mM NaF). One hundred micrograms of each protein sample were separated by SDS-PAGE (12% (*w/v*) acrylamide) and then blotted onto Hybond-P PVDF membranes (Amersham Biosciences, Freiburg, Germany) using a semi-dry transfer system. Membranes were blocked for 1 h at room temperature in 5% nonfat dry milk TBST (140 mM NaCl, 10 mM Tris, pH 7.6, 0.05% Tween-20) and probed overnight at 4 °C with primary antibodies against ID2 (C-20, sc-489, Santa Cruz Biotechnology) or p63 (4A4, sc-8431, Santa Cruz Biotechnology), which were diluted 200 times in 1% nonfat dry milk TBST solution. An HRP-conjugated antibody was used to probe β-actin (1/20000 dilution, A3854, Sigma-Aldrich) as a loading control on the same membranes. The blots were then washed and incubated with the respective HRP-conjugated secondary antibody (1/2000 dilution, anti-rabbit, 12–348; 1/2000 dilution, anti-mouse, 12–349, Millipore, CA) at room temperature for 1 h. Detection was carried out with the SuperSignal chemiluminescent system (Pierce).

Expression Profiles—The GEO database to analyze *ID2* expression in p63 knockdown expression profiles were obtained by colleagues in the world (38).

Luciferase Reporter Assay—HaCaT cells were seeded in 96-well plates the day before transfection at a density of 5000 cells/cm^2. Using jetSI-ENDO (PolyPlus Transfection), 120 ng of pID2-Luc2P plasmid was transfected in each well along with 10 nM siRNA and 5 ng of phRL-TK plasmid (Promega), which was used as an internal control of transfection. Luciferase activity was measured 48 h post-transfection using a dual-luciferase reporter assay system (Promega).

Chromatin Immunoprecipitation Experiment—ChIP experiments were carried out as described previously (39, 40). Briefly, growing HaCaT cells were fixed with formaldehyde and cross-linked chromatin was extracted, and subsequently fragmented by sonication into 1–2-kb fragments. The chromatin was then immunoprecipitated with a polyclonal antibody against p63α,

or a control anti-FLAG antibody. After washing and reverse crosslinking, enrichment of *ID2* promoter loci compared with a control loci were assessed on agarose gel after PCR amplification (see supplemental Table S3 for primer sequences). A Bio-Rad MyIQ single color thermal cycler and a SYBR Green PCR Master mix was used in all Q-PCR experiments. Specificity of products was monitored with a heat dissociation curve. Fold enrichment was calculated with the formula $2^{-\Delta\Delta Ct}$ where the Ct represented the threshold cycles of the input, the specific antibody and the negative antibody; a further normalization with the enrichment obtained on a negative genomic region (centromeric satellite 11) was applied. This double normalization reduced extent of enrichment but increased reproducibility.

Skin Sections Immunofluorescence—Skin sections were derived from biopsies of healthy donors. They were either fixed in formalin and embedded in paraffin wax or frozen prior to sectioning. Paraffin sections were dewaxed with two xylene washes, two 100% ethanol washes, two 70% ethanol washes and two distilled water washes (5 min at room temperature for each step). Samples were then unmasked in a 10 mM Tris, 1 mM EDTA, and 0.05% Tween 20 solution for 5 min at 85 °C. After blocking in 1× PBS and 10% goat serum, skin sections were incubated overnight with the primary antibodies: mouse anti-p63 (4A4, Dako) and rabbit anti-ID2 (Zymed Laboratories Inc.). After a 1-h incubation with Alexa-conjugated secondary antibodies (Invitrogen) and Hoechst dye, slides were mounted with 100 mM Tris and 70% glycerol.

Frozen skin sections were stored in optimal cutting temperature compound. Five microns skin sections were generated with a cryostat and frozen on polylysine glass slides (Menzel-Gläser) until used. After blocking in 1× PBS and 1% bovine serum albumin, skin sections were incubated overnight with the primary antibodies as for paraffin sections. IF with ID2 alone were performed with a Cy3-conjugated secondary antibodies (Jackson Immunoresearch) and mounted with Vectashield containing 1.5 μg/ml DAPI. Fluorescence was analyzed with a Leica confocal microscope.

RESULTS

siRNA Microarray Screen—To characterize repressors of *ID2* gene expression, we performed a large-scale RNAi-based loss-of-function screen using reverse transfection on siRNA microarrays coupled to a GFP reporter assay. A 2-kb fragment from the *ID2* promoter region was cloned upstream of the GFP coding sequence, and the resulting construct was transduced into the HaCaT human keratinocyte cell line. HaCaT cells stably expressing the *ID2*-promoter::GFP reporter construct (pID2-HaCaT cells) were reverse transfected on siRNA microarrays. The expression of GFP under control of the *ID2* promoter was monitored 72h after transfection by analysis of rGFP (the ratio of GFP-specific/DNA-specific fluorescence) (supplemental Fig. S1). We used a subset of 440 siRNA targeting 220 human genes; oncogenes, tumor suppressors and cell cycle regulators, from the Human Cancer siRNA Set v2 (Qiagen) targeting (supplemental Table S1).

The screening procedure is illustrated in supplemental Fig. S1. The images obtained contained both positive (GFP-targeted siRNA) and negative (scrambled siRNA) control spots, and as an example show three siRNA targeting new negative regulators of *ID2*, *NBN*, *p63*, and *RAD21* (Fig. 1*A*). A closer view of the spots clearly showed changes in GFP expression (Fig. 1*B*). Despite slight variations in cell number between spots, a significant decrease in the GFP-specific signal was observed within spots containing a GFP-targeted siRNA compared with spots containing scrambled siRNA. In contrast, a significant increase in GFP expression was observed in spots containing siRNA targeting either *NBN*, *p63* or *RAD21* (Fig. 1*B*). Moreover, the use of scrambled siRNA as a negative control showed that cell viability and GFP expression were not affected by reverse transfection of nonspecific siRNA, as indicated by the equal number of cells growing within spots and in the "transfection-free" area.

The distribution of fluorescence intensities over the siRNA microarrays typically showed proportionality between 532 nm and 635 nm, indicating that the GFP signal increased with cell number (Fig. 1*C*). The distribution of the negative control (scrambled siRNA) spots followed the global trend of all spots, dispersed along the *x* axis as a function of cell number. However, the 635 nm fluorescence signal in these spots was well-centered in the distribution, suggesting that GFP expression was not modulated in these cells. In contrast, the distribution of all but two positive controls (GFP-targeted siRNA) was shifted toward low fluorescence intensities (635 nm values), reflecting an efficient knockdown of GFP expression. The remainders of the spots were dispersed along the *x* axis of fluorescence intensity values, illustrating the necessity of normalizing GFP signal to cell number.

Each siRNA was processed independently, even when they targeted the same gene. siRNA having at least 3 unflagged features out of the quadruplicate on a given array were considered in the analysis. For each array, siRNA were ranked according to the median of the rGFP measurements. The reproducibility of this ranking was assessed across 3 independent microarrays for each siRNA, by calculating the median of percentile ranks per array (supplemental Fig. S1). The distribution of the median of percentile ranks for each siRNA exhibited a bi-modal shape (Fig. 1*D*). Effective siRNA were expected to rank at both tails of this distribution. The analysis procedure was validated with both negative and positive controls. Cells transfected with the GFP-targeted siRNA were systematically classified at the left side of the distribution, while negative control siRNA were scattered in the middle of this bi-modal distribution, as expected (Fig. 1*D*). A list of the top 6 ranking siRNA which consistently led to the induction of GFP after transfection, were considered to target potential repressors of *ID2* promoter activity (supplemental Table S2). Among them we identified 4 genes, *AURKB*, *NBN (NBS1)*, *p63*, and *RAD21* that we choose to further validate.

Validation of the Putative Repressors of ID2 Promoter Activity—Candidate *ID2* repressors were further validated by "forward" transfection in regular cell cultures. Semi-quantitative real-time PCR (qRT-PCR) analysis was first used to determine the extent of gene knock-down upon siRNA transfection. *P63*-, *RAD21*-, and *NBN*-targeted siRNA efficiently reduced the expression of corresponding gene (Fig. 2, *A*–*C*). Concomitantly, we validated effects of the siRNA on endogenous *ID2*

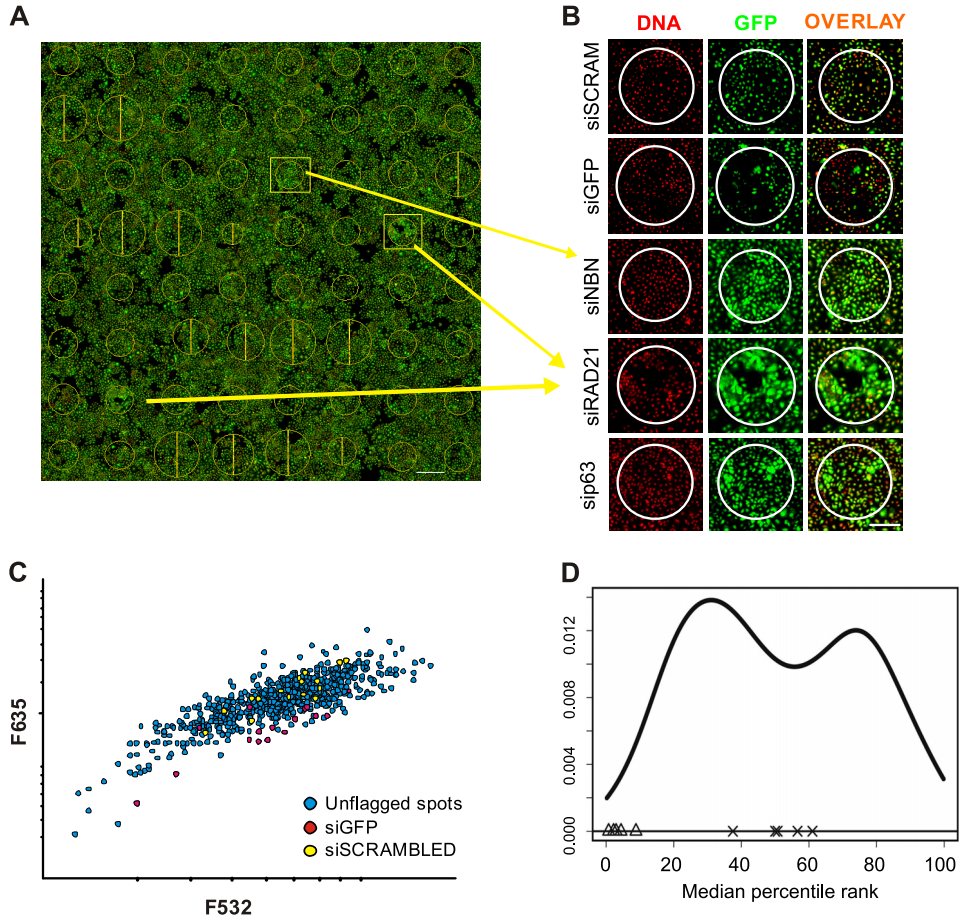

FIGURE 1. **siRNA microarray screen.** *A*, scan of a transfected arrays is presented, with cellular GFP appearing in *green*, and the DNA content stained in *red*. The *yellow circles* represent areas where specific siRNA was printed and where reverse transfection of cells occurred. Position and size of the *circles* were automatically calculated by the Genepix software that was used to analyze the data *B*, close-up view of the image presented in *A*. The green/red channels as well as the overlay are presented for the two controls and new putative *ID2* regulators. A decrease in GFP can be observed with the GFP-targeted siRNA compared with cells transfected with the scrambled siRNA. By contrast, *NBN- (NBS1), p63-*, and *RAD21*-targeting siRNA induced up-regulation of *ID2*-dependent GFP expression. Scale bar indicates 200 μm. *C*, scatter plot displaying distribution of F635 and F532 signal intensities for each spot in a given siRNA microarrays showed a linear increase of the GFP signal proportional to the number of cells estimated from DNA content. siGFP-targeted siRNA (*red*) and scrambled siRNA (*yellow*) are also indicated on the plot. *D*, distribution of the median of rankings among all replicated siRNA microarrays. The graph depicts the ranking-based non-parametric approach output for a batch of 4 replicate siRNA microarrays. The GFP-targeted siRNA spots (Δ) are consistently classified at the lower end of the distribution while scrambled siRNA (×) transfected cells are consistently ranked in the middle of the distribution, validating the strategy used for the analysis.

gene expression in HaCaT cells. The knockdown of *p63*, *NBN*, and *RAD21* increased the expression of endogenous *ID2* both at mRNA and protein levels (Fig. 2, *A–C*), consistent with the *ID2* promoter-dependent GFP modulations observed on siRNA microarrays. On the contrary we were not able to validate the effect of AURKB depletion on *ID2* expression (data not shown). Concordant results between the siRNA microarrays, qRT-PCR and Western blot analyses were obtained for the selected siRNA. This siRNA microarrays-mediated loss-of-function screen enabled the characterization of three new putative repressors of *ID2*. Interestingly two of them are involved in cell cycle checkpoint control. *NBN* participates in S-phase checkpoint pathway, while *RAD21* acts in establishing normal spindle-kinetochore interaction and is part of spindle checkpoint activation. Both genes are important to promote cell cycle progression and mitosis arrest. This result suggests that silencing *ID2* at transcript level would be necessary to promote cell cycle exit. However none of these proteins are transcription factor and probably act indirectly on *ID2* expression. Only p63, a member of the p53 gene family, is a well-known transcription factor that could act as a direct repressor of *ID2*.

p63 Represses ID2 Gene Expression in Adult Human Keratinocytes—Transfection of *p63*-targeted siRNA in HaCaT cells led to an effective knockdown of p63 both at the transcript (Fig. 2*A*) and protein levels (Fig. 3*A*), and with an induction of endogenous ID2 (Fig. 3*A*). Using an *ID2* promoter assay based on luciferase activity instead of GFP, we confirmed that p63 could regulate the *ID2* gene promoter activity in HaCaT cells (Fig. 3*B*). Two isoforms, TAp63 and ΔNp63, are functionally active in human keratinocytes. Although the specific role of these isoforms in epidermis development remains mostly unclear, ΔNp63 seems to be the main mediator of keratinocyte proliferation and differentiation, as this isoform is largely predominant in human keratinocytes (41). Interestingly, overexpression of either TAp63γ or ΔNp63α only slightly down-regulated *ID2* transcript level (Fig. 3*C*). This result suggests that, in physiological conditions, p63 would not suppress ID2 expression, but would rather prevent excessive transcription of it. We

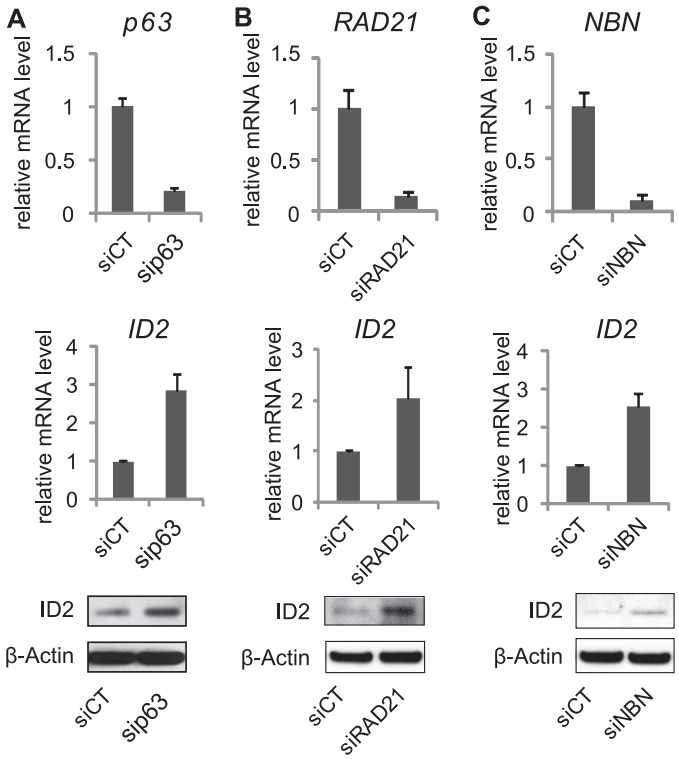

FIGURE 2. **Validation of the putative repressors of ID2.** Inhibition of p63 (*A*), RAD21 (*B*), and NBN (*C*) by siRNA, was quantified by RT-qPCR. Endogenous expression of ID2 was measured by RT-qPCR and immunoblot. Samples were extracted 48 h post-transfection from HaCaT cells, and error bars represent ± S.D.

also referenced the GEO database to analyze *ID2* expression in p63 knockdown expression profiles obtained by colleagues in the world. *p63* knockdown-dependent regulation of *ID2* was confirmed in HaCaT and other epithelial cells (Fig. 3*D*). The *p63* knockdown-dependent up-regulation of *ID2* was also observed in primary cultures of human keratinocytes (Fig. 3*E*). Finally, we studied the co-expression of ID2 and p63 mRNAs using a database containing normalized gene expression data on most of the human genes across 9783 tissue samples (42). If *p63* were an inducer of *ID2*, one would observe a positive linear regression between the two mRNA expression levels. On the contrary, if *p63* were a repressor of *ID2,* one would observe a negative linear regression. Actually, as demonstrated in Fig. 3*F*, when the relative expression level of p63 is above 600, that of *ID2* rarely exceeds 2000; *i.e.* the lower third. These expression data exquisitely confirm our molecular data and suggest that *p63* prevent excessive expression of *ID2*. Furthermore these data suggest that the regulation of *ID2* by *p63* occurs in many tissues. The maximum amplitude of variation observed for *ID2* expression in the skin expression profiles in the database was from 550 to 2,300 relative units of expression (supplemental Fig. S2), *i.e.* up to 4.2-fold, at most. The quartile distribution (25–75%) range of expression was from 900 to 1600, *i.e.* up to 1.8-fold, at most. Strikingly, our *ex vivo* molecular data fit well within these ranges of expression. Taken together, these results demonstrate that p63 acts as a repressor of *ID2* not completely suppressing *ID2* expression, but rather controlling it to prevent excessive expression of that gene in adult human keratinocytes.

ID2 Gene Repression by p63 Is Mediated by Direct Binding of p63 on the ID2 Promoter—To determine if p63 binds onto the *ID2* promoter, chromatin immunoprecipitation (ChIP) experiments were performed in growing HaCaT cells using two different α-p63-specific antibodies (43). P63 binding onto the ID2 promoter was detected by PCR (Fig. 4*A*). Two distinct regions of the *ID2* promoter, located 800 and 2500 bp upstream from the TSS, were enriched after p63 immunoprecipitation (IP) compared with the control (Fig. 4*B*). This suggests a direct binding of p63 onto *ID2* promoter in these two regions. Potential p63 binding sites within the promoter region of *ID2* were assessed using Genomatix software, which indicated three putative p63 binding sites at −754 bp, −2443 bp, and −2701 bp upstream of the first TSS (Fig. 4*C*). To study the function of each of these putative binding sites, increasing lengths of the promoter region that controls luciferase activity were deleted, and this deletion analysis showed that the −754 bp site was the most efficient in down-regulating *ID2* gene promoter activity (Fig. 4*D*). Finally, we engineered a short deletion of 7 nucleotides within the −754 p63 binding site and showed that this site mediated the p63-dependent repression of *ID2* gene promoter activity (Fig. 4*E*).

p63 and ID2 Proteins Expression in Human Epidermis and in Differentiating Primary Keratinocytes—The expression of p63 and ID2 proteins was monitored *in situ* in human skin sections. ID2 protein was detected in the epidermal basal layer, with very little presence in the spinous layer corresponding to the first stage of keratinocyte differentiation and high quantities in the granular layer, the terminal differentiation layer (Fig. 5, *A* and *B* and supplemental Fig. S3). Interestingly, ID2 was mainly nuclear in the basal layer and cytoplasmic in the granular layer (Fig. 5*B*). This is consistent with the subcellular location of ID2 in human skin cells both in the nucleus but not nucleoli and the cytoplasm (supplemental Fig. S3). p63 was expressed in the nuclei, very strongly in the basal layer, to a smaller extent in the spinous layer and could not be detected in the granular layer (Fig. 5, *A* and *C*). In the basal layer both proteins were expressed, while in the granular layer, the absence of p63 resulted in very high expression of ID2, thus confirming our molecular data (Fig. 5*A*). These *in vivo* results are again consistent with the role of p63 as a repressor of *ID2,* not abolishing its expression, but rather regulating it to prevent excessive expression of ID2.

We next monitored over 9 days *in vitro*, the *p63* and *ID2* transcript levels in differentiating primary keratinocytes. While the expression of Δ*Np63* constantly decreased over that period (Fig. 5*D*), *ID2* expression was more complex. It decreased at day 1, then slowly increased and finally remained constant after 5 days, when Δ*Np63* was almost no longer expressed (Fig. 5*E*). We also monitored the expression of keratin 1 (*K1*), a well characterized marker of early differentiation and of the basal-spinous switch in epidermis. *K1* expression level started to increase at day 2 and then continuously increased (Fig. 5*E*). Interestingly, *p63* and *ID2* expression patterns in differentiating keratinocytes modeled in a way the *in vivo* protein expression patterns in skin sections. Moreover, it confirmed once again that high Δ*Np63* expression level contains excessive *ID2* expression. Finally, we investigated the role of p63 and ID2 in

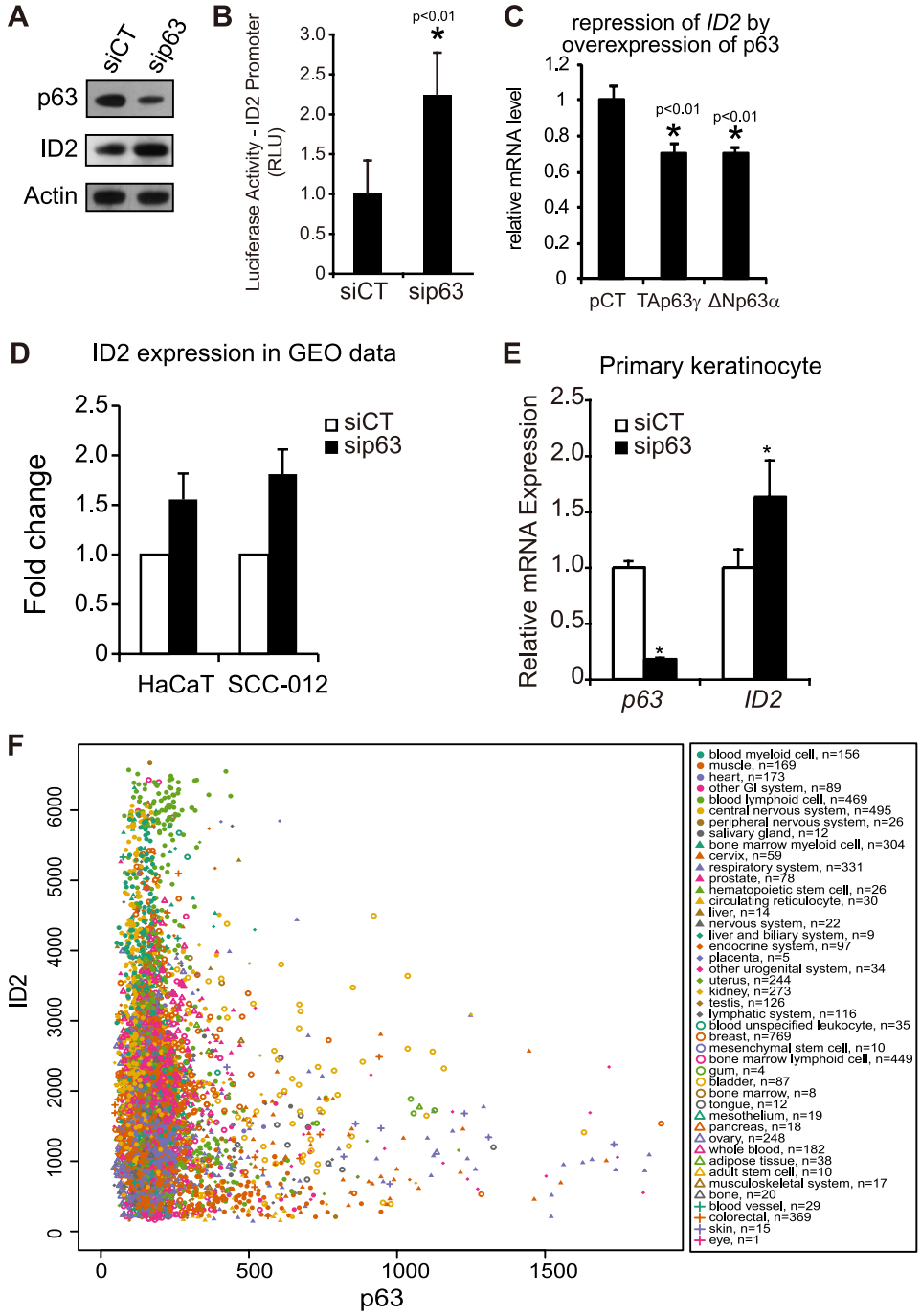

FIGURE 3. **p63 is a repressor of *ID2* in adult human keratinocytes.** *A*, an efficient knockdown of the p63 at protein level was observed by immunoblot and a concomitant up-regulation of ID2 when compared with control siRNA-transfected cells (siCT, control siRNA; siP63, p63-targeted siRNA). Actin was used as loading control. *B*, quantification of ID2 promoter-luciferase reporter activity in p63-deficient HaCaT cells. *Renilla* luciferase was used as internal control. Error bars indicate the ± S.D. (*, *t* test, $p < 0.01$, $n = 6$). *C*, overexpression of TAp63γ or ΔNp63α represses endogenous *ID2* expression. Error bars indicate the ± S.D. (*, *t* test, $p < 0.01$, $n = 3$). pCT was the control plasmid. *D*, data were analyzed from a comprehensive study including expression profiling in HaCaT and SCC-012 cells transfected with *p63* siRNA using the algorithm of the expression profiling database GEO (GSE4975) (38). The p63 depletion-dependent up-regulation of *ID2* was reported with three different probes in two cell lines, HaCaT and SCC-012. *E*, endogenous *ID2* is up-regulated consecutive to *p63* silencing in primary human keratinocytes. Error bars represent ± S.D. (*, *t* test, $p < 0.01$, $n = 3$). *F*, *in silico* co-expression analysis of *ID2* and *p63* mRNAs in normal and cancer human tissues present in the *in silico* transcriptomics database (42). The normalized expression levels of *ID2* are presented on *y* axis as a function of *p63* expression levels on *x* axis. The tissues and number of samples (*n*) are indicated in the *box*.

the keratinocyte commitment to differentiation. Functional studies were performed at day 2 in *in vitro* differentiation experiments as it is a key time in differentiation commitment, functionally equivalent to the transition between basal and spinous layers *in vivo*. While a 2.8-fold overexpression of *ID2* resulted in the inhibition of differentiation (Fig. 5*F*), knockdown of *p63* in HaCaT cells also inhibited differentiation as demonstrated by the reduced expression of *K1* (Fig. 5*G*). After 7 days the over-expression of *ID2* no longer inhibited *K1* expression (data not shown). Taken together our results suggest that the

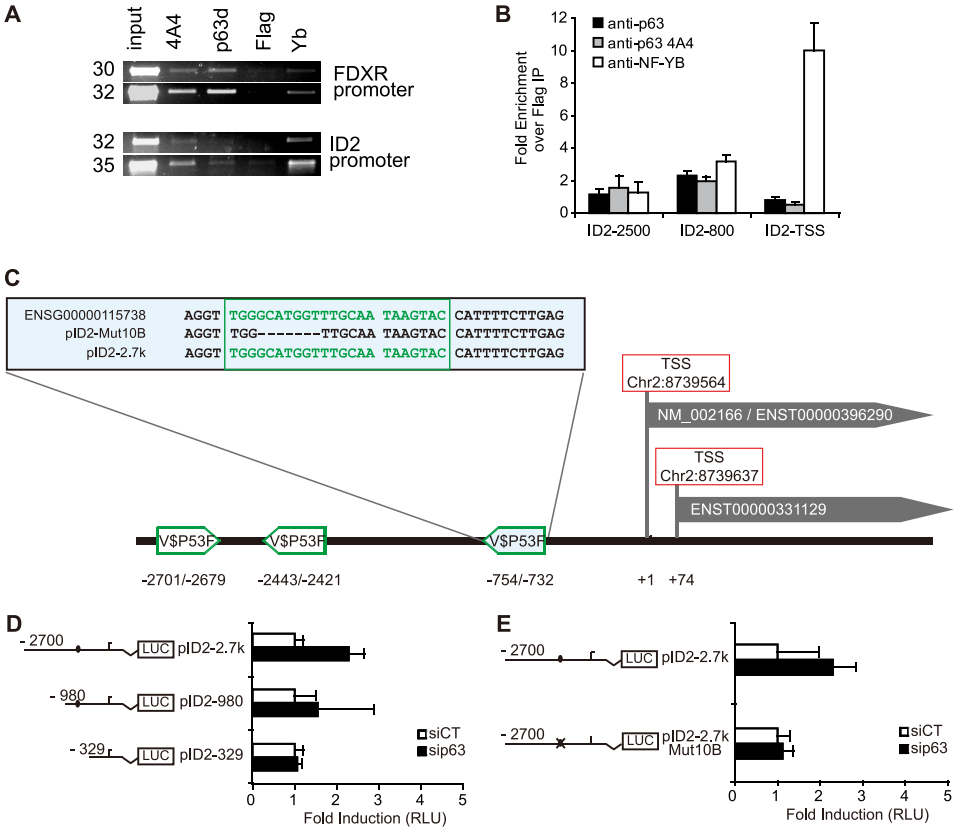

FIGURE 4. **p63 directly binds onto the promoter region of *ID2*.** *A*, ChIP was performed in growing HaCaT cells with polyclonal (*p63D*) or monoclonal (*4A4*) antibodies raised against p63, a flag (*Flag*) antibody as a negative control and NF-YB (*NF-YB*) directed antibody as a positive control. FDXR promoter was used as a positive control of p63 binding. Immunoprecipitated DNA was then further analyzed by quantitative-PCR. The set of primers used for ID2 the promoter amplification were the ID2–2500 (supplemental Table S3) *B*, a major enrichment was observed in a region around 800-bp upstream of the TSS with both anti-p63 antibodies, whereas another weaker binding occurred at around 2500 bp upstream of TSS. As expected, NF-YB binding was observed near the TSS. *C*, map of the *ID2* locus is displayed with two alternate TSS. Potential p63 binding sites (V$P53F) were identified within the *ID2* promoter sequence using Genomatix MatInspector tool at −2701, −2443, and −754 bp from the first TSS, respectively. The −754 binding site, present in both the wild-type gene (ENSG00000115738) and the reporter construct pID2–2.7k is detailed in the upper box. The deletion of this site obtained by directed mutagenesis of the reporter construct is also indicated (pID2Mut10B). *D* and *E*, HaCaT cells were cotransfected with *ID2* promoter-luciferase reporter of various lengths (pId2–2.7k, pId2–980, pId2–329) or mutant *ID2* promoter-luciferase reporter (pId2–2.7k Mut10B) together with a control reporter pRL-TK and either scrambled or p63-targeted siRNA. On schematic representations of the *ID2* promoter-reporter constructs, a *black circle* represents the putative −754 nt p63 binding sites, and a *crossed circle* is the mutated sequence. Luciferase activity (*RLU*) was defined as the ratio of firefly luciferase activity from *ID2* promoter-reporters relative to *Renilla* luciferase activity as the transfection control. Results are displayed as changes to induction of the luciferase activity after p63-targeted siRNA transfection compared with control siRNA. *Bars* and *brackets* indicate mean and standard deviation, respectively.

p63-dependent repression of *ID2* would be necessary to favor the keratinocyte cell cycle withdrawal and the onset of differentiation that occurs *in vivo* during the transition from basal to spinous layers. However, later in the differentiation process, in the granular layer, the expression of p63 seems too low to contain ID2 expression. The role of this high cytosolic expression of ID2 in the granular layer remains to be discovered.

DISCUSSION

To date, reports of *ID2* repressors are very scarce; only TGFβ had been identified as a partial and indirect repressor of *ID2* in epithelial cells (15). The RNAi/reporter screen in the present study enabled the characterization of 3 new direct and indirect repressors of *ID2*. Strikingly, we demonstrated that two genes playing a major role in cell cycle checkpoints, *NBN* in S-phase checkpoint and *RAD21* in spindle checkpoint, are leading to repression of *ID2*, which further highlighted the role for ID2 in cell cycle exit. Indeed, ID2 is a very unstable protein that is eliminated as cells withdraw from cycle (44). The anaphase promoting complex/cyclosome and its activator CDH1 (APC/C^{Cdh1}) targets ID2 for degradation through a destruction box motif (D box) that is conserved in ID1 and ID4 to couple cell cycle exit and axonal growth (44). We found that in addition to this ID2-targeted protein degradation mechanism, two genes, involved in the regulation of cell cycle withdrawal, *NBN* and *RAD21*, lead to a repression of *ID2* at the transcript level. These results emphasize the need to silence expression, at both the transcript and protein levels to prevent keratinocytes from re-entering the cell cycle. Indeed, due to the short half-life of ID2 protein (17), this dual level of repression might be particularly necessary. This finding is in agreement with our previous results, which show that *ID2* was necessary to revert double strand break-dependent cell-cycle arrest in human keratinocytes (13), but also with a recent report about the central role of ID2 within a generic transcription network regulating cell cycle in mouse and man (45). Together these results suggest a new potential role for ID2 in response to DNA damage and checkpoints exit.

We also show for the first time a p63-dependent direct repression of *ID2*. Based on *p63* knock-out mouse models, p63

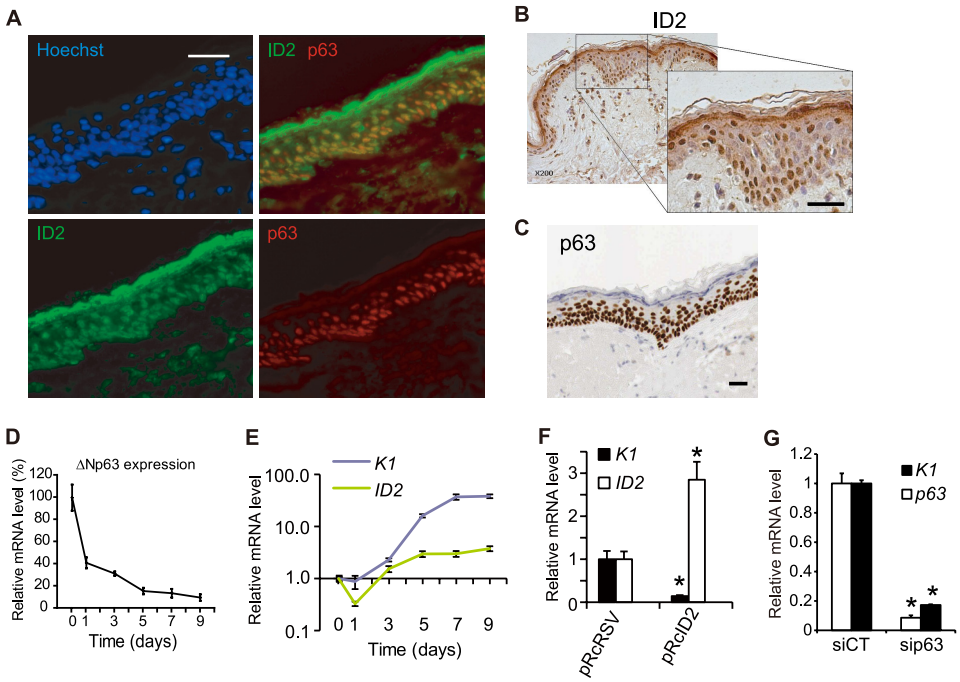

FIGURE 5. **Expression of ID2 and p63 in differentiating primary keratinocytes and in human skin.** *A*, expression of p63 and ID2 proteins in human skin. Sections of paraffin-embedded breast skin biopsies were stained with fluorescent p63-specific mAb (*red*), ID2-specific pAb (*green*), and Hoechst (*blue*). Scale bar is 100 μm. *B*, expression of ID2 in paraffin-embedded skin section was monitored by immunohistochemistry using DAB-stained ID2-specific pAb. Nuclei are stained by Hemalun and appeared in *blue*. Scale bar is 100 μm. *C*, p63-specific immunohistochemistry in paraffin-embedded skin sections extracted from the Human Protein Atlas database (57). Scale bar is 100 μm. *D*, expression of Δ*Np63* in differentiating primary keratinocytes. qRT-PCR analyses were perfomed with isoform-specific primers for Δ*Np63* (supplemental Table S3). *GAPDH* was used as an endogenous standard. *E*, *ID2* and keratin 1 (K1) expression were monitored by qRT-PCR in differentiating human primary keratinocytes. *F*, expression of *K1* and *ID2* was monitored after 2 days in differentiating HaCaT cell line with an overexpression of *ID2*. HaCaT Were also transformed with pRcRSV the control empty plasmid. (*, *t* test, $p < 0.01$, $n = 3$). *G*, Expression of *K1* and *p63* at 6 days post-transfection in differentiating HaCaT (*, *t* test, $p < 0.01$, $n = 3$). Error bars in all qRT-PCR graphs represent the standard deviation (S.D.) of triplicates.

was found to play an essential role in epidermal-mesenchymal interactions during embryonic development (34, 35). It is required for the stratification of the apical ectodermal ridge, for limb development and craniofacial development, and hence for the establishment and maintenance of stratified epithelia (46). p63-depleted keratinocytes exhibited impaired stratification and differentiation (41). Furthermore, p63 is crucial for the activation of the epithelial cell adhesion program (47) or to maintain the proliferative potential of stem cells (48). Taking into account the well-established roles of *ID2* in controlling epidermal homeostasis and cell fate in human keratinocytes (13–16), including its capacity to inhibit differentiation (6, 32, 49) the regulatory link that we observe between *p63* and *ID2* seems particularly interesting. Indeed, as it was recently suggested in an excellent review on epidermal homeostasis (50) that the identification of key genes downstream of p63 would provide important new insights into its roles in dynamic equilibrium of differentiation and proliferation. Our results show that *ID2* is one of these potential key genes acting downstream of p63 to control keratinocytes cell fate.

Six p63 proteins have been described, resulting from two promoters and alternative splicing (α, β, γ) at the 3′ end of the gene, with or without a sterile alpha motif (SAM) domain. The TA isoforms are structurally more like p53 and contain a transactivating domain while the ΔN isoforms lack this domain (51). The major isoform present in keratinocytes is ΔNp63α, and the genomic targets of this isoform have been partially described (52). Here we have shown that the ΔNp63α isoform was the most highly expressed in human keratinocytes and both isoform were able to slightly repress *ID2* gene promoter activity. Interestingly several studies recently demonstrated that ΔN isoforms are capable of transactivating genes through a proline-rich transactivation domain (53, 54).

Here we show that, siRNA-mediated knockdown of endogenous p63 represses ID2-inducible reporter gene activity in human cells. However, in apparent contradiction to these observations, upon transient overexpression of ΔNp63α *ex vivo* in human keratinocyte, we only observed a slight repression of the *ID2*-reporter construct. To explain these results we propose two hypotheses.

First, ΔNp63α could have a function in recruiting transcriptional repressors to *ID2* promoter region. Overexpression of p63 may lead to sequestration of such repressors, preventing excessive repression, as recently proposed on the role of p63 as a negative regulator of Wnt-induced transcription (55).

Second, it was recently shown that in cycling cells, p73 and p63 are bound to the p53-responsive elements (RE) present in the regulatory region of cell cycle regulating genes and compete with p53 to attach to these sites during the different phases of the cycle (56). Similarly, the binding of p63 to p53 RE upstream of *ID2* would not directly represses *ID2* but rather prevents action of positive regulators of *ID2.*

Nevertheless, the role of p63 as a negative *ID2*-regulator that we report here matches with the frequently observed down-regulation of p63 during tumor progression, when cancer cells adopt a more mesenchymal, invasive phenotype.

REFERENCES

1. Yokota, Y., and Mori, S. (2002) *J. Cell Physiol.* **190,** 21–28
2. Ruzinova, M. B., and Benezra, R. (2003) *Trends Cell Biol.* **13,** 410–418
3. Perk, J., Iavarone, A., and Benezra, R. (2005) *Nat. Rev Cancer* **5,** 603–614
4. Langlands, K., Yin, X., Anand, G., and Prochownik, E. V. (1997) *J. Biol. Chem.* **272,** 19785–19793
5. Ohtani, N., Zebedee, Z., Huot, T. J., Stinson, J. A., Sugimoto, M., Ohashi, Y., Sharrocks, A. D., Peters, G., and Hara, E. (2001) *Nature* **409,** 1067–1070
6. Norton, J. D., Deed, R. W., Craggs, G., and Sablitzky, F. (1998) *Trends Cell Biol.* **8,** 58–65
7. Lasorella, A., Noseda, M., Beyna, M., Yokota, Y., and Iavarone, A. (2000) *Nature* **407,** 592–598
8. Kleeff, J., Ishiwata, T., Friess, H., Büchler, M. W., Israel, M. A., and Korc, M. (1998) *Cancer Res.* **58,** 3769–3772
9. Stighall, M., Manetopoulos, C., Axelson, H., and Landberg, G. (2005) *Int. J. Cancer* **115,** 403–411
10. Alaminos, M., Gerald, W. L., and Cheung, N. K. (2005) *Pediatr. Blood Cancer* **45,** 909–915
11. Asirvatham, A. J., Carey, J. P., and Chaudhary, J. (2007) *Prostate* **67,** 1411–1420
12. Rollin, J., Bléchet, C., Régina, S., Tenenhaus, A., Guyétant, S., and Gidrol, X. (2009) *PLoS ONE* **4,** e4158
13. Baghdoyan, S., Lamartine, J., Castel, D., Pitaval, A., Roupioz, Y., Franco, N., Duarte, M., Martin, M. T., and Gidrol, X. (2005) *J. Biol. Chem.* **280,** 15836–15841
14. Memezawa, A., Takada, I., Takeyama, K., Igarashi, M., Ito, S., Aiba, S., Kato, S., and Kouzmenko, A. P. (2007) *Oncogene* **26,** 5038–5045
15. Kowanetz, M., Valcourt, U., Bergström, R., Heldin, C. H., and Moustakas, A. (2004) *Mol. Cell Biol.* **24,** 4241–4254
16. Rotzer, D., Krampert, M., Sulyok, S., Braun, S., Stark, H. J., Boukamp, P., and Werner, S. (2006) *Oncogene* **25,** 2070–2081
17. Tokuriki, A., Iyoda, T., Inaba, K., Ikuta, K., Fujimoto, S., Kumakiri, M., and Yokota, Y. (2009) *Carcinogenesis* **30,** 1645–1650
18. Scobey, M. J., Fix, C. A., and Walker, W. H. (2004) *J. Biol. Chem.* **279,** 16064–16070
19. Belletti, B., Prisco, M., Morrione, A., Valentinis, B., Navarro, M., and Baserga, R. (2001) *J. Biol. Chem.* **276,** 13867–13874
20. Rockman, S. P., Currie, S. A., Ciavarella, M., Vincan, E., Dow, C., Thomas, R. J., and Phillips, W. A. (2001) *J. Biol. Chem.* **276,** 45113–45119
21. Hacker, C., Kirsch, R. D., Ju, X. S., Hieronymus, T., Gust, T. C., Kuhl, C., Jorgas, T., Kurz, S. M., Rose-John, S., Yokota, Y., and Zenke, M. (2003) *Nat. Immunol.* **4,** 380–386
22. Aza-Blanc, P., Cooper, C. L., Wagner, K., Batalov, S., Deveraux, Q. L., and Cooke, M. P. (2003) *Mol. Cell* **12,** 627–637
23. Whitehurst, A. W., Bodemann, B. O., Cardenas, J., Ferguson, D., Girard, L., Peyton, M., Minna, J. D., Michnoff, C., Hao, W., Roth, M. G., Xie, X. J., and White, M. A. (2007) *Nature* **446,** 815–819
24. Kittler, R., Pelletier, L., Heninger, A. K., Slabicki, M., Theis, M., Miroslaw, L., Poser, I., Lawo, S., Grabner, H., Kozak, K., Wagner, J., Surendranath, V., Richter, C., Bowen, W., Jackson, A. L., Habermann, B., Hyman, A. A., and Buchholz, F. (2007) *Nat. Cell Biol.* **9,** 1401–1412
25. Ebert, B. L., Pretz, J., Bosco, J., Chang, C. Y., Tamayo, P., Galili, N., Raza, A., Root, D. E., Attar, E., Ellis, S. R., and Golub, T. R. (2008) *Nature* **451,** 335–339
26. Berns, K., Hijmans, E. M., Mullenders, J., Brummelkamp, T. R., Velds, A., Heimerikx, M., Kerkhoven, R. M., Madiredjo, M., Nijkamp, W., Weigelt, B., Agami, R., Ge, W., Cavet, G., Linsley, P. S., Beijersbergen, R. L., and Bernards, R. (2004) *Nature* **428,** 431–437
27. Paddison, P. J., Silva, J. M., Conklin, D. S., Schlabach, M., Li, M., Aruleba, S., Balija, V., O'Shaughnessy, A., Gnoj, L., Scobie, K., Chang, K., Westbrook, T., Cleary, M., Sachidanandam, R., McCombie, W. R., Elledge, S. J., and Hannon, G. J. (2004) *Nature* **428,** 427–431
28. Schlabach, M. R., Luo, J., Solimini, N. L., Hu, G., Xu, Q., Li, M. Z., Zhao, Z., Smogorzewska, A., Sowa, M. E., Ang, X. L., Westbrook, T. F., Liang, A. C., Chang, K., Hackett, J. A., Harper, J. W., Hannon, G. J., and Elledge, S. J. (2008) *Science* **319,** 620–624
29. Baghdoyan, S., Roupioz, Y., Pitaval, A., Castel, D., Khomyakova, E., Papine, A., Soussaline, F., and Gidrol, X. (2004) *Nucleic Acids Res.* **32,** e77
30. Lim, D. S., Kim, S. T., Xu, B., Maser, R. S., Lin, J., Petrini, J. H., and Kastan, M. B. (2000) *Nature* **404,** 613–617
31. Pati, D., Zhang, N., and Plon, S. E. (2002) *Mol. Cell Biol.* **22,** 8267–8277
32. Toyoda, Y., Furuya, K., Goshima, G., Nagao, K., Takahashi, K., and Yanagida, M. (2002) *Curr. Biol.* **12,** 347–358
33. Zhang, Y., Zhou, J., and Lim, C. U. (2006) *Cell Res.* **16,** 45–54
34. Mills, A. A., Zheng, B., Wang, X. J., Vogel, H., Roop, D. R., and Bradley, A. (1999) *Nature* **398,** 708–713
35. Yang, A., Schweitzer, R., Sun, D., Kaghad, M., Walker, N., Bronson, R. T., Tabin, C., Sharpe, A., Caput, D., Crum, C., and McKeon, F. (1999) *Nature* **398,** 714–718
36. Boukamp, P., Petrussevska, R. T., Breitkreutz, D., Hornung, J., Markham, A., and Fusenig, N. E. (1988) *J. Cell Biol.* **106,** 761–771
37. Livak, K. J., and Schmittgen, T. D. (2001) *Methods* **25,** 402–408
38. Barbieri, C. E., Tang, L. J., Brown, K. A., and Pietenpol, J. A. (2006) *Cancer Res.* **66,** 7589–7597
39. Viganò, M. A., Lamartine, J., Testoni, B., Merico, D., Alotto, D., Castagnoli, C., Robert, A., Candi, E., Melino, G., Gidrol, X., and Mantovani, R. (2006) *EMBO J.* **25,** 5105–5116
40. Viganò, M. A., and Mantovani, R. (2007) *Cell Cycle* **6,** 233–239
41. Truong, A. B., Kretz, M., Ridky, T. W., Kimmel, R., and Khavari, P. A. (2006) *Genes Dev.* **20,** 3185–3197
42. Kilpinen, S., Autio, R., Ojala, K., Iljin, K., Bucher, E., Sara, H., Pisto, T., Saarela, M., Skotheim, R. I., Björkman, M., Mpindi, J. P., Haapa-Paananen, S., Vainio, P., Edgren, H., Wolf, M., Astola, J., Nees, M., Hautaniemi, S., and Kallioniemi, O. (2008) *Genome Biol.* **9,** R139
43. Beretta, C., Chiarelli, A., Testoni, B., Mantovani, R., and Guerrini, L. (2005) *Cell Cycle* **4,** 1625–1631
44. Lasorella, A., Stegmüller, J., Guardavaccaro, D., Liu, G., Carro, M. S., Rothschild, G., de la Torre-Ubieta, L., Pagano, M., Bonni, A., and Iavarone, A. (2006) *Nature* **442,** 471–474
45. Ravasi, T., Suzuki, H., Cannistraci, C. V., Katayama, S., Bajic, V. B., Tan, K., Akalin, A., Schmeier, S., Kanamori-Katayama, M., Bertin, N., Carninci, P., Daub, C. O., Forrest, A. R., Gough, J., Grimmond, S., Han, J. H., Hashimoto, T., Hide, W., Hofmann, O., Kawaji, H., Kubosaki, A., Lassmann, T., van Nimwegen, E., Ogawa, C., Teasdale, R. D., Tegnér, J., Lenhard, B., Teichmann, S. A., Arakawa, T., Ninomiya, N., Murakami, K., Tagami, M., Fukuda, S., Imamura, K., Kai, C., Ishihara, R., Kitazume, Y., Kawai, J., Hume, D. A., Ideker, T., and Hayashizaki, Y. (2010) *Cell* **140,** 744–752
46. McKeon, F. (2004) *Genes Dev.* **18,** 465–469
47. Carroll, D. K., Carroll, J. S., Leong, C. O., Cheng, F., Brown, M., Mills, A. A., Brugge, J. S., and Ellisen, L. W. (2006) *Nat. Cell Biol.* **8,** 551–561
48. Senoo, M., Pinto, F., Crum, C. P., and McKeon, F. (2007) *Cell* **129,** 523–536
49. Simbulan-Rosenthal, C. M., Trabosh, V., Velarde, A., Chou, F. P., Daher, A., Tenzin, F., Tokino, T., and Rosenthal, D. S. (2005) *Oncogene* **24,** 5443–5458
50. Fuchs, E. (2009) *Cell Stem Cell* **4,** 499–502
51. Irwin, M. S., and Kaelin, W. G. (2001) *Cell Growth Differ.* **12,** 337–349
52. Pozzi, S., Zambelli, F., Merico, D., Pavesi, G., Robert, A., Maltère, P., Gidrol, X., Mantovani, R., and Vigano, M. A. (2009) *PLoS ONE* **4,** e5008
53. Helton, E. S., Zhu, J., and Chen, X. (2006) *J. Biol. Chem.* **281,** 2533–2542
54. Liu, G., Nozell, S., Xiao, H., and Chen, X. (2004) *Mol. Cell Biol.* **24,** 487–501
55. Drewelus, I., Göpfert, C., Hippel, C., Dickmanns, A., Damianitsch, K., Pieler, T., and Dobbelstein, M. (2010) *Cell Cycle* **9,** 580–587
56. Lefkimmiatis, K., Caratozzolo, M. F., Merlo, P., D'Erchia, A. M., Navarro, B., Levrero, M., Sbisa, E., and Tullo, A. (2009) *Cancer Res.* **69,** 8563–8571
57. Berglund, L., Björling, E., Oksvold, P., Fagerberg, L., Asplund, A., Al-khalili Szigyarto, C., Persson, A., Ottosson, J., Wernérus, H., Nilsson, P., Lundberg, E., Sivertsson, A., Navani, S., Wester, K., Kampf, C., Hober, S., Pontén, F., Uhlén, M. (2008) *Mol. Cell. Proteomics* **10,** 2019–2027